The Boundary of Lithium Plating in Graphite Electrode for Safe Lithium-Ion Batteries

Wenlong Cai, Chong Yan, Yu-Xing Yao, Lei Xu, Xiao-Ru Chen, Jia-Qi Huang and Qiang Zhang*

Abstract: Uncontrolled Li plating in graphite electrodes endangers battery life and safety, driving tremendous efforts aiming to eliminate Li plating. Herein we systematically investigate the boundary of Li plating in graphite electrode for safe lithium-ion batteries. The cell exhibits superior safety performance than that with Li dendrites by defining the endurable amount of uniform Li plating in graphite anode. The presence of „dead Li" can be eliminated owing to the uniform distribution of Li plating, and the average Coulombic efficiency for deposited Li during reversible plating/stripping process is decoupled as high as about 99.5 %. Attributing to the limited Li plating with superior Coulombic efficiency, the $LiNi_{0.5}Mn_{0.3}Co_{0.2}O_2$ | graphite cell achieves a high capacity retention of 80.2 % over 500 cycles. This work sheds a different light on further improving the fast-charging capability, low-temperature performance, and energy density of practical lithium-ion batteries.

Introduction

Lithium-ion batteries are gradually dominating our daily life from consumer electronics to battery electric vehicles. Graphite has long been the irreplaceable commercial anode material ascribing to its high stability and low cost.[1–3] However, exploring lithium-ion batteries with stable cycling as well as superior safety performance is strongly considered in many emerging applications.[4,5]

It is acknowledged that the operating potential (ca. 0.1 V vs. Li/Li$^+$) of graphite anode locates above 0 V, therefore only Li$^+$ intercalate into graphite materials in terms of thermodynamics. Nevertheless, various polarizations including ohmic drop, charge transfer overpotential, and concentration overpotential, drive anode potential across the threshold of Li plating.[6,7] Similar to the Li metal electrode, the deposited Li metal in graphite anode often presents in the form of needles or dendrites.[8,9,10] Owing to their intrinsic reactive nature, the unstable deposited Li exhibits high reactivity with electrolyte to gradually form a redundant solid electrolyte interphase (SEI) layer and consume active lithium.[11,12] During the de-lithiation process, Li starts to strip from the roots of Li dendrites, which interrupts conductive contacts to the substrate, resulting in the generation of „dead Li".[12,13] Moreover, continuous cycling creates more „dead Li", resulting in an increasement of cell resistance which in turn promotes further Li plating. The vicious cycle of Li plating leads to an endless reduction of Coulombic efficiency (CE) and attenuation of battery life.[6,14] More seriously, the steady growth of Li dendrites can pierce the porous separators to short cathode and anode in a working battery, which is prone to undergo thermal runaway and even cell explosion.[1,15,16] On the other hand, the reactions between plated Li and electrolyte are exothermic. The accumulation of excessive heat further leads to fire or explosion even no internal short-circuits are produced.[17]

Regulating Li plating in graphite electrode has been proved to be an effective method to improve the energy density of a battery. Both Cui et al. and Dahn et al. successively investigated a novel anode system of hybrid graphite/lithium metal anode.[2,18] These strategies reveal compelling results in improving the energy density, demonstrating the significant concepts of structure optimization and electrolyte additives for hybrid lithium-ion/ lithium metal operation. Note that the well-established commercial electrolyte consists of carbonate solvents for routine lithium-ion batteries is not suitable for the reversible plating/stripping of Li metal.[19] The above-mentioned electrolyte typically results in dendritic Li metal deposits, along with the generation of „dead Li" and an unsatisfactory low CE (< 80 %).[20] Therefore, the solvent-derived SEI seems to be a terrible choice in reducing the loss of metal Li, which is detrimental for prolonged cycling.[21] Fortunately, localized high concentration electrolyte (LHCE) has been applied with the advantage of a high capability to construct robust SEI to suppress Li dendrites, achieving chunky Li deposition with ultrahigh Li reversibility (CE > 99 %).[10,15,22] Furthermore, LHCE renders good compatibility with graphite anode, enabling a uniform anion-derived SEI and exhibiting fast-charging potential in working batteries.[23–25] Therefore, the highly reversible Li plating/stripping efficiency makes it possible for in-depth exploration of the behavior of hybrid graphite/lithium metal anode. There have been some mysteries focus on the following issues that need to be solved: 1) how much Li metal deposits in commercial graphite electrode is endurable

[*] Dr. W. L. Cai, Dr. C. Yan, Y.-X. Yao, X.-R. Chen, Prof. Q. Zhang
Beijing Key Laboratory of Green Chemical Reaction Engineering and Technology, Department of Chemical Engineering
Tsinghua University
Beijing 100084 (China)
E-Mail: zhang-qiang@mails.tsinghua.edu.cn

L. Xu, Prof. J.-Q. Huang
Advanced Research Institute of Multidisciplinary Science
Beijing Institute of Technology
Beijing 100081 (China)

Supporting information and the ORCID identification number(s) for the author(s) of this article can be found under:
https://doi.org/10.1002/anie.202102593.

for long-term cycling, 2) what is the safety performance of the graphite electrode with Li plating, 3) what is the pragmatic CE for Li metal reversible plating/stripping on the lithiation graphite surface?

Herein, we attempt to address the safety concerns of Li metal deposits in graphite electrode. By regulating the uniform distribution of plated Li, the limited capacity of Li plating is defined as 25% of lithiation graphite. Safety performance tests, including overcharge and nail penetration tests of pouch cells, further confirm the controllable trends in temperature changes with the occurring of controlled Li plating. By subtracting the CE of graphite electrode during the intercalation process, the average CE for deposited metal Li plating/stripping on the lithiation graphite host is decoupled as high as ca. 99.5%. The longevity cycling performance of $LiNi_{0.5}Mn_{0.3}Co_{0.2}O_2$ (NMC 532) | graphite cell with a controlled Li plating in graphite electrode is investigated to validate the feasibility in practical lithium-ion batteries.

Results and Discussion

For lithium-ion batteries based on conventional concentration electrolyte (CCE), metal Li starts to electroplate on graphite surface once the overpotential of conversion reaction is lower than that of intercalation reaction and then forms Li dendrites mostly on the top surface (Supporting Information, Figure S1a–e). The existence of Li dendrites results in the accumulation of undesired „dead Li" after several cycles, which has been one of the main culprits of battery performance degradation. LHCE has been successfully employed in lithium metal batteries.[9,10,25] Herein we prepare a kind of LHCE that is consisting of most anions in the primary solvation sheath (Supporting Information, Figure S2). This is expected to generate inorganic species dominated SEI on graphite surface (Supporting Information, Figures S3 and S4).[23] Benefiting from the thin and robust SEI film, excess Li plating is uniformly distributed across the whole graphite electrode. (Supporting Information, Figure S1f–j). The uniform distribution of Li metal is expected to generate no „dead Li" during repeated cycling under the premise of superior safety performance.

The pristine SEI layer cannot be maintained when excessive Li plating on graphite surface. This induces undesirable side effects, including the formation of „dead Li" and the generation of Joule heat to deteriorate the safety performance of the working cells. Accordingly, it is imperative to initially quantify the optimum amount of Li plating in graphite anode. An ex-situ scanning electron microscopy (SEM) analysis was conducted to record the morphology evolution of graphite electrode after galvanostatic Li intercalation and plating at a low current density of 0.1 C (1 C = 372 mAh g^{-1}) using Li metal as a counter electrode. As depicted in Figure 1a, a reasonable capacity of 367 mAh g^{-1} is obtained above 0 V, corresponding to the formation of LiC_6. When the voltage was further discharged below 0 V, a long plateau was observed which can be regarded as the plating of Li metal in graphite electrode. Based on the capacity of LiC_6 (367 mAh g^{-1}), the amount of plated Li is defined (LiC_6 +
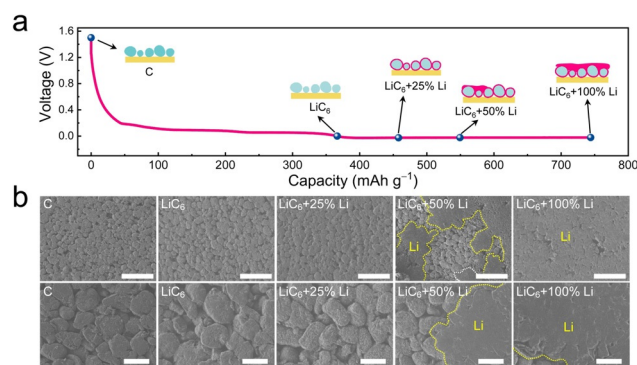

Figure 1. Characterization of the morphology evolution of graphite electrode upon Li intercalation and plating. a) The electrochemical curve for Li intercalation and plating in graphite electrode and b) corresponding SEM images at various stages. The scar bars for the upper and below row in (b) are 100 and 20 μm, respectively.

25% Li: 460 mAh g^{-1}, LiC_6 + 50% Li: 550 mAh g^{-1}, LiC_6 + 100% Li: 740 mAh g^{-1}). It can be seen that little morphology change can be observed after Li full intercalation into graphite particles (Figure 1b). When extra quarter Li plating in graphite electrode (LiC_6 + 25% Li), there is no considerable morphology evolution but only some tiny particles on graphite particles. However, the deposited Li metal emerges to cover parts of graphite particles when the amount of Li plating doubles (LiC_6 + 50% Li). Furthermore, almost all graphite particles are overwhelmed by external Li plating after the capacity further doubles (LiC_6 + 100% Li). It is worth noting that excessive Li plating presents as bulk Li deposition without Li dendrite, which is important to achieve a comparatively high plating/stripping efficiency of metal Li. Nevertheless, even the formation of small amounts of „dead Li" impedes the subsequent intercalation/de-intercalation process of active graphite materials. Therefore, the endurable amount of Li plating in graphite electrode should be less than 50% of the capacity of lithiation graphite.

Safety performance is the most important factor for lithium-ion batteries in consumer electronics and battery electric vehicles. Both overcharge and nail penetration tests were conducted based on practical pouch cells to investigate the thermal performance of the cells with extra Li plating in lithiation graphite anode. The overcharge tests were firstly performed on the cells at 80% state of charge (SOC) and a full lithiation graphite anode was defined as 100% SOC. The thermal distributions of cells were monitored by an IR camera during the test, while both surface temperatures were also recorded. As depicted in Figure 2a–c and the Supporting Information, Movie S1, the surface temperatures of the cells with uniform Li plating and Li dendrites are essentially same at 125% SOC. Nevertheless, the temperature of the cell with Li dendrites starts to increase rapidly at 130% SOC and generates flames and explosion after 159% SOC. For comparison, the cell with uniform Li plating has a broad SOC range (147% SOC) to maintain stable surface temperature, and the temperature at 158% SOC is just comparative to that of the cell with Li dendrites at 145% SOC. Until 167% SOC, the cell with uniform Li plating produces too much heat and then explodes. Besides, the highest explosion temper-
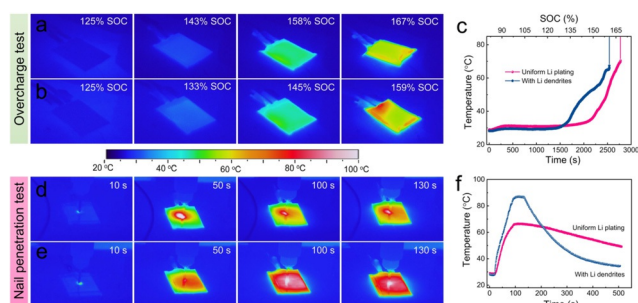
Figure 2. Safety performance tests of the cells with uniform Li plating and Li dendrites. IR images of the cell (a) with uniform Li plating and (b) with Li dendrites at different stages, and corresponding (c) temperature-time curves during overcharge test. IR images of the cell (d) with uniform Li plating and (e) with Li dendrites at different times, and corresponding (f) temperature-time curves during nail penetration test.

ature of the cell with uniform Li plating is about 500°C (Supporting Information, Figure S5a), which is lower than that of the cell with Li dendrites (600°C), indicative of much less accumulated heat in the process. Noted that the surface temperature of the cell with uniform Li plating begins to show a slow warming trend at 130% SOC (Supporting Information, Figure S5b), while the surface temperature at 125% SOC is the same as that at 100% SOC. These results indicate that controlling the capacity of Li plating in graphite electrode no more than 25% of the capacity of lithiation graphite is reasonable.

To further substantiate the superior safety performance of the cell with uniform Li plating, a sharp stainless-steel nail was penetrated through the center of the cells with an extra 25% Li plating in graphite electrodes. The IR camera was also used to monitor the heat distribution. As shown in Figure 2d–f and the Supporting Information, Movie S2, the penetrated nail results in short circuit inside the cells with a large amount of released Joule heat. Significantly, the temperature close to the puncture region increases immediately which is defined by the shorting resistance of cells.[26] On the other hand, the rise of the surface temperature of pouch cells is determined by the intrinsic thermal properties of cells. Benefiting from the robust SEI, the plated metal Li with uniform distribution exhibits lower reactivity with working electrolyte to produce less heat, while Li dendrites will burst out SEI to produce side effects. Consequently, the highest surface temperature of the cell with uniform Li plating is about 66°C, which is much smaller than that of the cell with Li dendrites (90°C). As a comparison, the highest surface temperatures of the cells with LHCE and CCE at 100% SOC are 65°C and 78°C (Supporting Information, Figure S6), respectively. These results demonstrate the superior safety performances of the cell with uniform Li plating in graphite electrode comparing with that of Li dendrites.

The distribution of Li elements during reversible plating/stripping process was further studied through time-of-flight secondary ion mass spectrometry (TOF-SIMS) analysis. The evolution of Li element in the graphite electrode with LHCE during discharging/charging process was firstly investigated (Figure 3a–f; Supporting Information, Figure S7a–c). Fig-
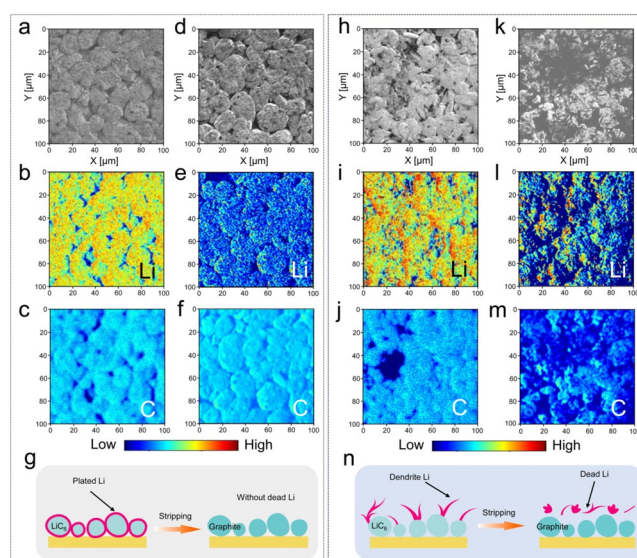

Figure 3. Characterization of graphite electrodes during reversible plating and stripping process. a),d) TOF-SEM, b),e) Li TOF-SIMS mapping, and c),f) C TOF-SIMS mapping of the graphite electrodes (a–c) with Li plating and (d–f) after Li stripping and de-intercalation in LHCE system. g) Representation of Li plating and stripping in the graphite electrode with uniform Li plating. h),k) TOF-SEM, i),l) Li TOF-SIMS mapping, and j),m) C TOF-SIMS mapping of the graphite electrodes (h–j) with Li plating and (k–m) after Li stripping and de-intercalation in CCE system. n) Representation of Li plating and stripping in the graphite electrode with Li dendrites.

ure 3a and the Supporting Information, Figure S7a elucidate the absence of Li dendrites after the intercalation and plating process. Specifically, the signals of Li elements (Figure 3b; Supporting Information, Figure S7b) are highly consistent with that of C element (Figure 3c; Supporting Information, Figure S7c), demonstrating the uniform distribution of Li element on graphite surface. After the de-lithiation process (Figure 3d–f; Supporting Information, Figure S7d–f), the signal of Li element becomes weak but is still uniformly distributed, which is contributed by the uniform SEI layer and negligible „dead Li". The uniform distribution of Li plating in graphite electrode generates few „dead Li" during cycling, as schematically illustrated in Figure 3g, which is favorable for long-term cycling. For comparison, the behavior of Li plating/stripping in the graphite electrode with CCE was also investigated. As revealed in Figure 3h–j and the Supporting Information, Figure S7g–i, the deposited Li presents as dendrites locating among graphite particles. The misalignment element mappings of Li and C further validate that Li plating is not uniform in the graphite electrode with CCE. Figure 3k–m and the Supporting Information, Figure S7j–l further reveal the inconsistent distribution of Li and C elements after the de-lithiation process, which is contributed by the formation of „dead Li". As a result, Li plating presenting as dendrites prefers to produce undesired „dead Li" during cycling (Figure 3n). Furthermore, Li plating and stripping on bare Cu substrate was performed with LHCE. Notably, Cu substrate with the rough surface was applied for Li deposition, as much as possible to avoid the effect of surface area. As shown in the Supporting Information,

Figure S8, the chunky Li on Cu is not uniform and also prone to generate „dead Li" after stripping. The overpotential of Li metal plating in the graphite electrode with LHCE is lowest than that in the graphite electrode with CCE and on Cu substrate with LHCE (Supporting Information, Figure S9). In short, the lithiophilicity lithiation graphite,[27] apart from the functional electrolyte, is a key factor for uniform nucleation and growth of metallic Li.

The long-term electrochemical stability of uniform Li plating in graphite electrode was evaluated in graphite | Li cells. The areal capacity of the graphite electrode is ca. 2.2 mAh cm^{-2}. Figure 4a and b exhibit typical galvanostatic voltage profiles of the graphite electrodes with and without uniform Li plating in LHCE at 0.23 mA cm^{-2}. Three obvious plateaus for Li intercalation locating at 0.20, 0.12, and 0.08 V can be observed for the graphite electrode without Li plating. The corresponding initial Coulombic efficiency (ICE) is 94.6%. When Li metal further deposits on the lithiation graphite surface, another long plateau emerges below 0 V, which can be taken as Li plating potential. The ICE for the graphite electrode with uniform Li plating is 94.5%, which is lower than that without Li plating but outclass that of the graphite electrode with Li dendrites (91.5%; Supporting Information, Figure S10). After the first two formation cycles at 0.23 mA cm^{-2}, cells were cycled at 0.70 mA cm^{-2} in the following cycles. As shown in Figure 4c, the CE for the graphite electrode with uniform Li plating increases to 99%

in the initial five cycles and sustains over 99% in the following 100 cycles. The coincided voltage profiles of Li intercalation/plating and stripping/de-intercalation after the initial cycle demonstrate stable reversible cycling (Supporting Information, Figure S11). The CE can climb to 99% after 10 cycles for the graphite electrode with Li dendrites, however, quickly decays to below 80%. When the amount of uniform deposited Li doubles (Supporting Information, Figure S12), the CE reduces to less than 98% after 80 cycles, suggesting excessive chunky Li plating results in accumulation of „dead Li" to deteriorate the long-term cycling performance, further confirming the importance of defining the endurable capacity of Li plating.

Owing to the reversibility of Li plating/stripping on lithiation graphite, it is necessary to decouple the CE for deposited metal Li during the intercalation/conversion process. By subtracting the CE of the graphite electrode without Li plating, the pragmatic CE for metal Li can be estimated according to the following equation:

$$CE_{\text{Li plating}} = 1 - \left[\left(1 - CE_{\text{LiC}_6 + \text{Li plating}}\right) - \frac{\left(1 - CE_{\text{LiC}_6}\right)C_{\text{LiC}_6}}{C_{\text{LiC}_6 + \text{Li plating}}}\right] \qquad (1)$$

where $CE_{\text{LiC}_6 + \text{Li plating}}$ and $C_{\text{LiC}_6 + \text{Li plating}}$ are reversible CE and capacity for the graphite electrode with Li plating, while CE_{LiC_6} and C_{LiC_6} are reversible CE and capacity for the graphite electrode without Li plating. Correspondingly, the average CE for metal Li is calculated as 99.5% for 100 cycles (Figure 4d), indicating the ultrahigh reversibility of uniform Li plating in graphite electrode. For comparison, the average CE for metal Li in dendrite morphology is only 92.2% (Supporting Information, Figure S13). Besides, the long-term reversible plating and stripping process on Cu substrate was also investigated based on LHCE (Supporting Information, Figure S14). A regular average CE of 98.4% is obtained with the same capacity of Li deposition. These results demonstrate that the uniform distribution of Li plating in graphite electrode is able to achieve ultrahigh reversibility.

NMC 532 | graphite cell with an N/P ratio below one was further assembled to monitor the feasibility of uniform Li plating in graphite anode during long-term cycling. Initially, the electrochemical stability window of LHCE was tested by linear scan voltammetry (LSV) in a Li | Al cell. As can be seen from the Supporting Information, Figure S15, the decomposition of electrolytes for both CCE and LHCE occurs when the voltage is over 4.5 V. Then NMC 532 with an areal capacity of ca. 2.4 mAh cm^{-2} was employed as cathode, while the areal capacity of graphite electrode is ca. 2.2 mAh cm^{-2}. The higher areal capacity of cathode than that of anode ensures that Li metal deposits in graphite electrode after full charging. However, the capacity of Li metal in anode should be controlled under 25% of that of lithiation graphite. Therefore, the rate performances of NMC 532 cathode and graphite anode were, respectively, investigated in the cells coupled with Li metal as counter electrodes. This can provide the appropriate current density for long-term limited Li plating in NMC 532 | graphite cells. A home-made Li reference electrode was inserted into graphite | Li cell to manipulate the electrochemical window of graphite electrode,
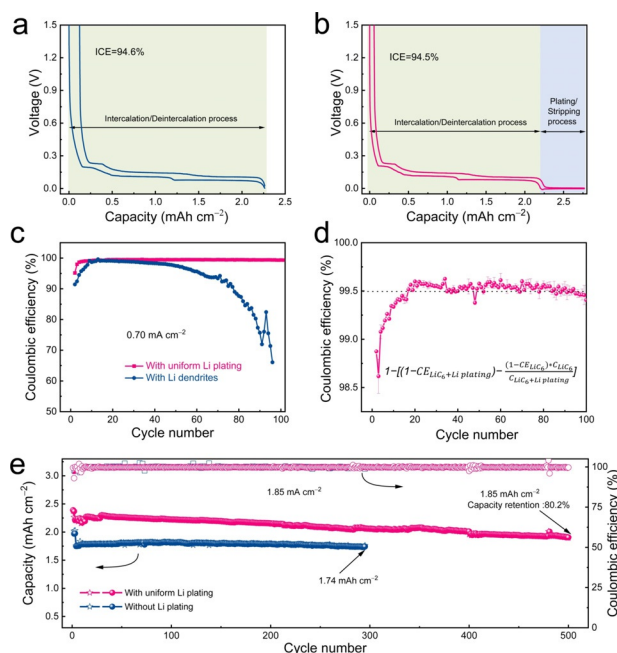

Figure 4. Electrochemical performance of the graphite electrode with Li plating in graphite | Li half cells and NMC 532 | graphite cell. Voltage profiles of the graphite electrodes (a) without and (b) with uniform Li plating at a current density of 0.23 mA cm^{-2}. c) Coulombic efficiency of the graphite electrodes with uniform Li plating or Li dendrites over cycling. d) Coulombic efficiency of metal Li with uniform distribution in graphite electrode during reversible plating and stripping process. e) Long-term cycling performance of the NMC 532 | graphite cells with uniform Li plating and without Li plating in LHCE at 1.85 mA cm^{-2} between 2.8–4.3 V.

avoiding the larger overpotential of Li counter electrode results in undervaluing the rate capability of graphite electrode in routine two-electrode device.[28] Figure S16 exhibits that the areal capacities of NMC 532 and graphite reduce with the rising of current density, while the reduction tendency for graphite is more obvious. Specifically, the capacity ratio of NMC 532 to graphite (P/N) at the constant current stage decreases from 1.08 at 0.46 mA cm^{-2} to 1.45 at 3.46 mA cm^{-2} (Supporting Information, Figure S17). A P/N ratio of 1.22 at 1.85 mA cm^{-2} is enough to meet the requirement of limiting the amount of Li plating under 25 %. Based on this consideration, the NMC 532 | graphite cell was designed to operate at 1.85 mA cm^{-2} for long-term cycling. Figure 4e reveals that the full cell delivers a capacity of 1.85 mAh cm^{-2} after 500 cycles with a capacity retention of 80.2 %, which is still higher than that of the cell without Li plating in LHCE (1.74 mAh cm^{-2} after 300 cycles). Besides, the differential capacity dQ/dV versus voltage plots indicate that distinct Li plating occurs throughout the electrochemical cycling (Supporting Information, Figure S18). These results suggest that uniform Li plating in graphite electrode enables long-term stable cycling of safe lithium-ion batteries.

In general, Li plating is the main culprit of fast-charging and low-temperature lithium-ion batteries.[5,29] The generation of Li plating in dendritic form has long been thought to be avoided, or else it will cause battery short circuit and lead to thermal runaway and even cell explosion. Interestingly, this work sheds a different light on understanding the conundrum of Li plating. By defining the boundary of the graphite electrode with safe Li plating, the fast-charging capability and low-temperature performance of practical lithium-ion batteries may be further improved. Besides, this work offers another avenue to boost the energy density of lithium-ion batteries by regulating the capacity ratio of cathode and anode or replenishing more lithium sources to the cathode materials.

Conclusion

The boundary of the graphite electrode with uniform Li plating was systematically investigated. The results reveal that batteries can keep safe condition while Li plating is controlled below 25 % of the total capacity of lithiated graphite, along with a high average CE of 99.5 % for the stripping/plating process. Ascribing to the uniform distribution of metal Li, the cell exhibits superior safety performance comparing with mussy Li dendrites and few „dead Li" in graphite electrode during repeated cycling. The NMC 532 | graphite full cell with a controlled Li plating can operate over 500 cycles with a large capacity retention of 80.2 %. In contrast to the routine wisdom that aims to inhibit Li plating, this work offers another avenue to recycle waste Li plating for long-term cycling, which can be used as a guide to further improve the energy density of lithium-ion batteries as well as fast-charging capability and low-temperature performance.

[1] W. Cai, Y. X. Yao, G. L. Zhu, C. Yan, L. L. Jiang, C. He, J. Q. Huang, Q. Zhang, *Chem. Soc. Rev.* **2020**, *49*, 3806–3833.

[2] Y. Sun, G. Zheng, Z. W. Seh, N. Liu, S. Wang, J. Sun, H. R. Lee, Y. Cui, *Chem* **2016**, *1*, 287–297.

[3] C. Yan, Y.-X. Yao, W.-L. Cai, L. Xu, S. Kaskel, H. S. Park, J.-Q. Huang, *J. Energy Chem.* **2020**, *49*, 335–338; Y. K. Kim, Y. Kim, J. Bae, H. Ahn, Y. Noh, H. Han, W. B. Kim, *J. Energy Chem.* **2020**, *48*, 285–292.

[4] J. Asenbauer, T. Eisenmann, M. Kuenzel, A. Kazzazi, Z. Chen, D. Bresser, *Sustainable Energy Fuels* **2020**, *4*, 5387–5416; S. S. Zhang, *ChemElectroChem* **2020**, *7*, 3569–3577.

[5] A. Tomaszewska, Z. Chu, X. Feng, S. O'Kane, X. Liu, J. Chen, C. Ji, E. Endler, R. Li, L. Liu, Y. Li, S. Zheng, S. Vetterlein, M. Gao, J. Du, M. Parkes, M. Ouyang, M. Marinescu, G. Offer, B. Wu, *eTransportation* **2019**, *1*, 100011.

[6] Q. Liu, C. Du, B. Shen, P. Zuo, X. Cheng, Y. Ma, G. Yin, Y. Gao, *RSC Adv.* **2016**, *6*, 88683–88700.

[7] T. Waldmann, B.-I. Hogg, M. Wohlfahrt-Mehrens, *J. Power Sources* **2018**, *384*, 107–124; Y. X. Yao, C. Yan, Q. Zhang, *Chem. Commun.* **2020**, *56*, 14570–14584.

[8] C. Yan, Y. X. Yao, X. Chen, X. B. Cheng, X. Q. Zhang, J. Q. Huang, Q. Zhang, *Angew. Chem. Int. Ed.* **2018**, *57*, 14055–14059; *Angew. Chem.* **2018**, *130*, 14251–14255; R. Xu, Y. Xiao, R. Zhang, X. B. Cheng, C. Z. Zhao, X. Q. Zhang, C. Yan, Q. Zhang, J. Q. Huang, *Adv. Mater.* **2019**, *31*, 1808392.

[9] S. Chen, J. Zheng, D. Mei, K. S. Han, M. H. Engelhard, W. Zhao, W. Xu, J. Liu, J. G. Zhang, *Adv. Mater.* **2018**, *30*, 1706102.

[10] J. Fu, X. Ji, J. Chen, L. Chen, X. Fan, D. Mu, C. Wang, *Angew. Chem. Int. Ed.* **2020**, *59*, 22194–22201; *Angew. Chem.* **2020**, *132*, 22378–22385.

[11] S. S. Zhang, *J. Electrochem. Soc.* **2020**, *167*, 060527.

[12] X. B. Cheng, R. Zhang, C. Z. Zhao, Q. Zhang, *Chem. Rev.* **2017**, *117*, 10403–10473.

[13] X. B. Cheng, R. Zhang, C. Z. Zhao, F. Wei, J. G. Zhang, Q. Zhang, *Adv. Sci.* **2016**, *3*, 1500213.

[14] Y. Liu, Y. Zhu, Y. Cui, *Nat. Energy* **2019**, *4*, 540–550; W. Cai, C. Yan, Y.-X. Yao, L. Xu, R. Xu, L.-L. Jiang, J.-Q. Huang, Q. Zhang, *Small Struct.* **2020**, *1*, 2000010; X.-G. Yang, T. Liu, Y. Gao, S. Ge, Y. Leng, D. Wang, C.-Y. Wang, *Joule* **2019**, *3*, 3002–3019.

[15] Y. Jie, X. Ren, R. Cao, W. Cai, S. Jiao, *Adv. Funct. Mater.* **2020**, *30*, 1910777.

[16] M. Li, M. Feng, D. Luo, Z. Chen, *Cell Rep. Phys. Sci.* **2020**, *1*, 100212; J. Hou, L. Lu, L. Wang, A. Ohma, D. Ren, X. Feng, Y. Li, Y. Li, I. Ootani, X. Han, W. Ren, X. He, Y. Nitta, M. Ouyang,

Nat. Commun. **2020**, *11*, 5100; E. J. McShane, A. M. Colclasure, D. E. Brown, Z. M. Konz, K. Smith, B. D. McCloskey, *ACS Energy Lett.* **2020**, *5*, 2045 – 2051; D. Ren, H. Hsu, R. Li, X. Feng, D. Guo, X. Han, L. Lu, X. He, S. Gao, J. Hou, Y. Li, Y. Wang, M. Ouyang, *eTransportation* **2019**, *2*, 100034.

[17] Y. Ye, L. H. Saw, Y. Shi, K. Somasundaram, A. A. O. Tay, *Electrochim. Acta* **2014**, *134*, 327 – 337.

[18] C. Martin, M. Genovese, A. J. Louli, R. Weber, J. R. Dahn, *Joule* **2020**, *4*, 1296 – 1310.

[19] N. Piao, X. Ji, H. Xu, X. Fan, L. Chen, S. Liu, M. N. Garaga, S. G. Greenbaum, L. Wang, C. Wang, X. He, *Adv. Energy Mater.* **2020**, *10*, 1903568.

[20] F. Ding, W. Xu, G. L. Graff, J. Zhang, M. L. Sushko, X. Chen, Y. Shao, M. H. Engelhard, Z. Nie, J. Xiao, X. Liu, P. V. Sushko, J. Liu, J. G. Zhang, *J. Am. Chem. Soc.* **2013**, *135*, 4450 – 4456; S.-K. Jeong, H.-Y. Seo, D.-H. Kim, H.-K. Han, J.-G. Kim, Y. B. Lee, Y. Iriyama, T. Abe, Z. Ogumi, *Electrochem. Commun.* **2008**, *10*, 635 – 638.

[21] J. Qian, W. A. Henderson, W. Xu, P. Bhattacharya, M. Engelhard, O. Borodin, J. G. Zhang, *Nat. Commun.* **2015**, *6*, 6362.

[22] X. Fan, X. Ji, L. Chen, J. Chen, T. Deng, F. Han, J. Yue, N. Piao, R. Wang, X. Zhou, X. Xiao, L. Chen, C. Wang, *Nat. Energy* **2019**, *4*, 882 – 890; Y. Yamada, J. Wang, S. Ko, E. Watanabe, A. Yamada, *Nat. Energy* **2019**, *4*, 269 – 280.

[23] L. L. Jiang, C. Yan, Y. X. Yao, W. Cai, J. Q. Huang, Q. Zhang, *Angew. Chem. Int. Ed.* **2021**, *60*, 3402 – 3406; *Angew. Chem.* **2021**, *133*, 3444 – 3448.

[24] H. Jia, Y. Xu, S. D. Burton, P. Gao, X. Zhang, B. E. Matthews, M. H. Engelhard, L. Zhong, M. E. Bowden, B. Xiao, K. S. Han, C. Wang, W. Xu, *ACS Appl. Mater. Interfaces* **2020**, *12*, 54893 – 54903.

[25] X. Cao, Y. Xu, L. Zhang, M. H. Engelhard, L. Zhong, X. Ren, H. Jia, B. Liu, C. Niu, B. E. Matthews, H. Wu, B. W. Arey, C. Wang, J.-G. Zhang, W. Xu, *ACS Energy Lett.* **2019**, *4*, 2529 – 2534.

[26] X. Huang, J. Xue, M. Xiao, S. Wang, Y. Li, S. Zhang, Y. Meng, *Energy Storage Mater.* **2020**, *30*, 87 – 97.

[27] T. Chen, W. Jia, Z. Yao, Y. Liu, X. Guan, K. Li, J. Xiao, H. Liu, Y. Chen, Y. Zhou, D. Sun, J. Li, *Electrochem. Commun.* **2019**, *107*, 106535.

[28] S. S. Zhang, *J. Electrochem. Soc.* **2020**, *167*, 100510.

[29] S. S. Zhang, *InfoMat* **2020**, *2*, 942 – 949.